



p-Type conducting transparent characteristics of delafossite Mg-doped CuCrO₂ thin films prepared by RF-sputtering

Antoine Barnabé, Yohan Thimont, Maëva Lalanne, Lionel Presmanes,
Philippe Tailhades

► To cite this version:

Antoine Barnabé, Yohan Thimont, Maëva Lalanne, Lionel Presmanes, Philippe Tailhades. p-Type conducting transparent characteristics of delafossite Mg-doped CuCrO₂ thin films prepared by RF-sputtering. Journal of Materials Chemistry C, 2015, vol. 3 (n° 23), pp. 6012-6024. 10.1039/c5tc01070e . hal-01167277

HAL Id: hal-01167277

<https://hal.science/hal-01167277>

Submitted on 24 Jun 2015

HAL is a multi-disciplinary open access archive for the deposit and dissemination of scientific research documents, whether they are published or not. The documents may come from teaching and research institutions in France or abroad, or from public or private research centers.

L'archive ouverte pluridisciplinaire **HAL**, est destinée au dépôt et à la diffusion de documents scientifiques de niveau recherche, publiés ou non, émanant des établissements d'enseignement et de recherche français ou étrangers, des laboratoires publics ou privés.



Open Archive TOULOUSE Archive Ouverte (OATAO)

OATAO is an open access repository that collects the work of Toulouse researchers and makes it freely available over the web where possible.

This is an author-deposited version published in : <http://oatao.univ-toulouse.fr/>
Eprints ID : 14014

To link to this article : doi: 10.1039/c5tc01070e
URL : <http://dx.doi.org/10.1039/c5tc01070e>

To cite this version : Barnabé, Antoine and Thimont, Yohan and Lalanne, Maëva and Presmanes, Lionel and Tailhades, Philippe *p-Type conducting transparent characteristics of delafossite Mg-doped CuCrO₂ thin films prepared by RF-sputtering*. (2015) Journal of Materials Chemistry. C, vol. 3 (n° 23). pp. 6012-6024. ISSN 2050-7526

Any correspondence concerning this service should be sent to the repository administrator: staff-oatao@listes-diff.inp-toulouse.fr

p-Type conducting transparent characteristics of delafossite Mg-doped CuCrO_2 thin films prepared by RF-sputtering

A. Barnabé,* Y. Thimont, M. Lalanne, L. Presmanes and P. Tailhades

The growth of technologically relevant compounds, Mg-doped CuCrO_2 delafossite thin films, on a quartz substrate by radio-frequency sputtering is reported in this work. The deposition, performed at room temperature, leads to a nanocrystalline phase with extremely low roughness and high density. Delafossite characteristic diffraction peaks were obtained as a function of the thermal treatment under primary vacuum. The electrical conductivity was optimized until 1.6 S cm^{-1} with an optical transmittance of 63% in the visible range by a 600°C annealing treatment under primary vacuum applied for 4 h. The transport properties were analyzed by Seebeck and Hall measurement, integrated spectrophotometry and optical simulation. These measurements highlighted degenerated semiconductor behavior using a hopping mechanism with a high hole concentration (10^{21} cm^{-3}) and a low mobility ($0.2 \text{ cm}^2 \text{ V}^{-1} \text{ s}^{-1}$). The direct optical bandgap of 3.3 eV has been measured according to Tauc's relationship. A refractive index of 2.3 at a wavelength of 1100 nm has been determined by spectroscopic ellipsometry and confirmed by two independent modellings of the optical transmittance and reflectance spectra. All these p-type TCO optoelectronic characteristics have led to the highest Haacke's figure of merit ($1.5 \times 10^{-7} \Omega^{-1}$) reported so far for such delafossite materials.

1. Introduction

Metal oxides are a class of materials showing one of the greatest ranges of properties and are more and more attractive for various applications. A metal–oxygen bond is strong so that oxides have a combination of a high heat of formation and a wide band gap. The wide-bandgap oxide semiconductors also called Transparent Conducting Oxides (TCOs), which combine electrical conductivity and optical transparency in a single material, are of particular interest.^{1,2} Therefore, TCO thin films are used as transparent electrodes in numerous technological applications including photovoltaic cells, flat panel displays, electromagnetic shielding devices, transparent heat sources and light emitting diodes.³ The majority and most popular TCOs currently available are n-type electron conductors. A p-type TCO has only been reported in 1997 for copper-based delafossite material CuAlO_2 .⁴ Since then, a number of promising wide bandgap p-type hole conductor materials have been found as a consequence of material exploration efforts following the design concept.^{5–9} Many studies over the last few years have led to the description of a number of p-type TCOs based on copper-based delafossite CuMO_2 oxides with $M = \text{Ga},^{10,11} \text{In},^{12} \text{Y},^{13}$ and Sc^{14}

for instance. Among them, CuCrO_2 based film prepared by radio frequency sputtering reaches a conductivity of 220 S cm^{-1} , which is the highest conductivity in p-type TCOs but with a limited optical transmittance in the visible region.¹⁵

In addition, some delafossite based CuMO_2 films have been used for application in transparent diode and UV-emitting diode devices¹⁰ with various n-type TCO counterparts. Realization of such a p/n-transparent hetero-junction makes it possible to investigate the possibility of invisible circuits based on transparent oxides,^{16,17} which are not feasible with n-type materials alone.

To achieve this aim from an application standpoint, a lot of difficulties have to be solved. First, it is necessary to be able to deposit the resultant material as a thin film on a transparent substrate. This has been already published using different deposition techniques and a large range of deposition conditions. However, the main TCO performance of these p-type thin film materials still needs improvements to, *in fine*, reach that of their n-type TCO counterparts. Second, proper control of the substrate temperature over the entire process sequence is required and may become an important issue for realistic applications since conventional or flexible substrates are required. For the CuMO_2 thin film, only very few data concerning the development of this class of materials at low temperature, *i.e.* below 450°C , have been published among all the references.¹⁸ This is explained by the fact that the development of this phase requires high

temperatures and strict conditions of preparation to be pure. The use of high temperatures needed for the successful crystallization of delafossite phases requires the use of heat-resistant substrates, which are relatively expensive. In addition, stabilization of monovalent noble metal cation A(I) in delafossite A(I)M(III)O₂ is not always possible under such conditions due to the natural tendency of this cation to decompose before forming reaction starts.

Among CuMO₂ systems with various M-cations and appropriate dopants, magnesium-doped CuCrO₂ films show conductivity greater than many other p-type TCOs, suitable band gaps and undergo quite low temperature processing. Hence, Mg-doped CuCrO₂ films are considered as one of the most potential candidates for opto-electronic applications.^{15,19} On top of that, the CuCrO₂ based material has also been studied for its antibacterial,²⁰ catalytic and photo-catalytic,^{21–24} magnetic,^{25–27} thermoelectric,^{28–32} multiferroic and magneto-electric^{33,34} properties, and applications in sensors,³⁵ photovoltaic cells³⁶ and batteries.³⁷

The synthesis and complete optical and electrical characterization of Mg-doped CuCrO₂ delafossite thin film using a radio-frequency sputtering technique is reported in this paper. In addition to previous work done on CuFeO₂¹⁸ it contributes to a better understanding of the complex reactions involved during the delafossite phase formation, in order to develop a versatile method for preparing thin films with oxide structure on copper-based delafossite CuMO₂ at relatively low temperature.

2. Materials and methods

Preparation of Mg-doped CuCrO₂ sputtering target material

Due to the very limited Mg²⁺ solubility range in the delafossite CuCrO₂ structure and then to prevent the precipitation of a secondary spinel phase which can affect the physical properties,^{26,38,39} the Mg content in Mg-doped CuCrO₂ was fixed to 3at% in this study. Polycrystalline CuCr_{0.97}Mg_{0.03}O₂ powder (denoted as Mg-doped CuCrO₂ in the manuscript) was prepared by grinding and mixing the starting commercial oxides, Cu₂O, Cr₂O₃ and MgO. The stoichiometric oxide mixture was treated at 900 °C for 10 h in an ambient nitrogen atmosphere and cooled down to room temperature. After it was reground, the mixture was reheated

for a further 10 h period. X-Ray diffraction (XRD) measurements performed using a Bruker D4 Endeavor X-ray diffractometer (copper radiation $\lambda_{\text{CuK}_{\alpha 1}} = 1.5405 \text{ \AA}$ and $\lambda_{\text{CuK}_{\alpha 2}} = 1.5445 \text{ \AA}$) showed a rhombohedral $R\bar{3}m$ delafossite phase with traces of magnesiochromite (Fig. 1) in good agreement with the very limited Mg²⁺ solubility range in CuCr_{1-x}Mg_xO₂.²⁶

The lattice parameters determined by the Rietveld method implemented in the Fullprof/WinPlotR program are $a = 2.9755(2) \text{ \AA}$ and $c = 17.091(3) \text{ \AA}$. In comparison with the undoped CuCrO₂ phase elaborated under the same experimental conditions where $a = 2.9742(2) \text{ \AA}$ and $c = 17.090(3) \text{ \AA}$,⁴⁰ a slight increase of the lattice parameter could be observed. This supports the partial integration of the magnesium species on the octahedral-site of the delafossite structure as it agrees well with the increase of the average ionic radius as chromium with $r(\text{Cr}^{3+}_{\text{Coord.VI}}) = 0.615 \text{ \AA}$ is replaced by magnesium with $r(\text{Mg}^{2+}_{\text{Coord.VI}}) = 0.720 \text{ \AA}$.

The polycrystalline delafossite powder was then pressed into a sputtering target of 10 cm in diameter and sintered at 1200 °C for 10 h in air. The relative density of the target was about 60%. XRD measurements carried out on a small representative pellet showed no foreign phases.

Preparation of Mg-doped CuCrO₂ thin film material

To produce desired thin films, the target assembly was attached to an Alcatel A450 Radio Frequency (RF) magnetron sputtering chamber. Prior to film deposition, pre-sputtering by argon plasma for 10 min was performed to remove surface contamination. Pre-cleaned fused quartz microscope substrates (25 × 25 mm, $\approx 1 \text{ mm}$ thick from Electron Microscopy Sciences Ref #72250-01) placed on a water-cooled sample holder were used. The deposition parameters summarized in Table 1 were optimized in terms of RF-power, magnetron, internal gas pressure and target to substrate distance, in order to maintain the nominal oxygen stoichiometry of the target constant thanks to previous work on CuFeO₂ thin film materials.^{18,41} Under these conditions the average deposition rate deduced from thickness measurements done by both surface profilometry and X-ray reflectometry was equal to 8.5 nm min^{-1} . Films with thicknesses in the range of 50 to 300 nm were deposited. Effective Mg-doping

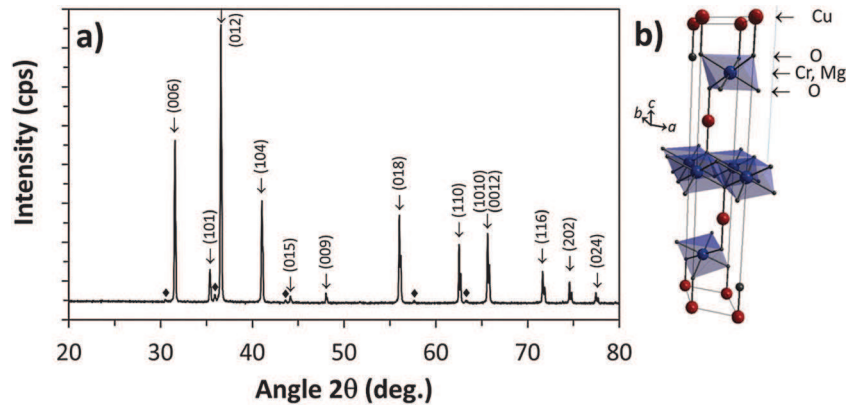


Fig. 1 (a) XRD pattern of the Mg-doped CuCrO₂ target. Traces of magnesiochromite are indicated by the \blacklozenge symbol. (b) Schematic representation of the delafossite structure.

Table 1 Process parameters for the deposition of delafossite Mg-doped CuCrO₂ by RF-sputtering

Target material	3at% Mg-doped CuCrO ₂
Substrate	Fused quartz
Power (W cm ⁻²)	0.9
Magnetron	Yes
Argon pressure <i>P</i> (Pa)	0.5
Target to substrate distance <i>d</i> (cm)	5

of the films was confirmed by electron probe micro-analysis (EPMA) using a Cameca SX 50 apparatus. From a minimum of ten measurements performed on films deposited on a silicon substrate, 0.7–0.8 atomic percent was obtained for the Mg content over the whole species (Cu + Cr + Mg + O). Expressed over the (Cr + Mg) content, it corresponds to an overall Mg-doping level of 3 atomic percent identical to the target composition.

The as-deposited films deposited on quartz substrates have been annealed for 4 h under primary vacuum at various temperatures ranging from 450 to 800 °C, to obtain the delafossite Mg-doped CuCrO₂ material.

Characterization

The structural properties of the films were investigated on 300 nm thick films by $\alpha = 1^\circ$ Grazing Incidence XRD (GIXRD) at room temperature and Temperature dependent XRD (TXRD). GIXRD was performed using a Siemens D5000 diffractometer equipped with a Bruker Sol-X detector. TXRD was performed using a Bruker D8 diffractometer in Bragg–Brentano θ – θ geometry equipped with a Bruker LynxEye 1D detector and an Anton Paar HTK1200N temperature chamber. In all cases, copper radiations were used as the X-ray source ($\lambda_{\text{CuK}\alpha 1} = 1.5405 \text{ \AA}$ and $\lambda_{\text{CuK}\alpha 2} = 1.5445 \text{ \AA}$).

The microstructure of the films was observed using a Jeol JSM-6400 field emission gun Scanning Electron Microscope (SEM) and a Nanoscope III Dimension 3000 Atomic Force Microscope (AFM). SEM and AFM surface views were analyzed using the Gwyddion software.⁴²

The electrical resistivity was measured using a Signatone four-point probe measurement unit. A Versalab Quantum Design Physical Properties Measurement System (PPMS) with an applied external field of 3 T was used for Hall measurements. A home-made room temperature Seebeck measurement device with gold probe contacts, adapted to the thin film geometry, was used for thermoelectric characterization.

The optical characteristics of thin films were investigated in the 300 to 1100 nm wavelength range using a Bentham PVE300 UV/Visible/IR integrated spectrophotometer, and then the spectra were modeled using the SCOUT software.⁴³ The ellipsometry technique has been used for the determination of the optical index. Measurements were carried out using a Jobin-Yvon/Horiba Uvisel spectroscopic ellipsometer (SE), in the 350 to 1000 nm spectral range. Ellipsometry data were recorded at an incidence angle of 70 degrees and were analyzed using the Delta-Psi 2 software (shell version 2.9). A sample stack structure (quartz/film/surface layer) was employed to extract the optical constants (*n* and *k*) of thin films.

3. Results and discussion

Structural analysis

The as-deposited thin film is amorphous according to XRD measurements (Fig. 2a). For this sample, no dominant diffraction peak could be observed because of the nanocrystalline nature of films as previously observed in such similar systems with Cr^{15,44} and Fe.¹⁸

Heat treatments have then been carried out up to 800 °C in order to highlight the phases, which could be crystallized or formed. The TXRD patterns recorded in Bragg–Brentano geometry in the 450 to 800 °C temperature range are displayed in Fig. 2a. Such treatments were carried out under primary vacuum to avoid oxidation of the pristine phase. Actually, a thermal treatment under an air atmosphere above 450 °C (TXRD done in this work but not shown here) leads to the formation of spinel CuCr₂O₄ with concomitant appearance of tenorite CuO in good agreement with previous reports.⁴⁵

From the TXRD diffractograms and for $T > 500 \text{ °C}$, a main broad and secondary diffraction peaks can be identified at $2\theta \approx 36^\circ$ and $\approx 62^\circ$, *i.e.* with $d_{hkl} \approx 2.5 \text{ \AA}$ and $\approx 1.5 \text{ \AA}$, respectively. It is difficult to match one particular phase among CuCrO₂, Cu₂O, and Cr₂O₃ with these TXRD patterns due to the overlap of the main diffraction peaks, the geometry and temperature chamber contributions and thermal expansion. However, the splitting of

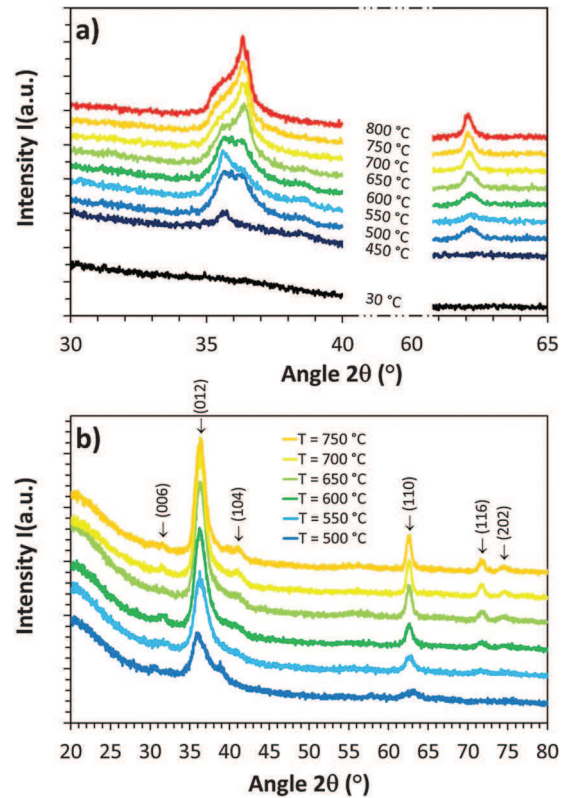


Fig. 2 XRD patterns of 300 nm thick Mg-doped CuCrO₂ films. (a) *In situ* TXRD patterns registered in θ – θ Bragg–Brentano geometry at various temperatures in the range of 30 to 800 °C under primary vacuum and (b) $\alpha = 1^\circ$ GIXRD patterns registered at room temperature after similar *ex situ* annealing treatment.

the broad main peak located at around 36° into two peaks at higher and lower 2θ values with a concomitant increase and decrease of their intensities, respectively, is in good agreement with the (012) and (101) Bragg reflections of the Mg-doped CuCrO_2 phase. The secondary peak located at $2\theta \approx 62^\circ$ also belongs to the delafossite-type structure with the (110) reflection.

From $\alpha = 1^\circ$ GIXRD measurements carried out at room temperature on annealed samples in the same temperature range (Fig. 2b), the (012) and (110) peaks could be more finely located at 36.5 and 62.7° in the 2θ range. Additional characteristic peaks belonging to the delafossite-type Mg-doped CuCrO_2 are also highlighted at $2\theta \approx 31.5, 41.0, 71.9$ and 74.9° and correspond to the (006), (104), (116) and (202) Bragg peaks, respectively.

All the XRD results consequently suggested that the samples annealed above 500°C were composed of delafossite-type Mg-doped CuCrO_2 . The lattice parameters $a = 2.959(3) \text{ \AA}$, $c = 17.06(9) \text{ \AA}$ and $V = 129.36 \text{ \AA}^3$ of the CuCrO_2 thin film determined from GIXRD pattern matching refinement on the sample annealed at 750°C are in good agreement with bulk Mg-doped CuCrO_2 data.

Despite the high anisotropic character of the delafossite structure and in contrast to previous studies where normal or highly c -axis polycrystalline delafossite films were obtained by various methods and/or conditions (sol-gel,^{45–47} chemical solution deposition⁴⁸ and pulsed laser deposition⁴⁹), this structural characterization indicates that the (00 l) reflection of the

delafossite structure is always very weak. This result was already reported in the literature for such CuCrO_2 films^{15,44,50,51} and could be correlated with the oxygen stoichiometry of the growing phases.

In this work, the use of non-reactive magnetron RF sputtering yields the Mg-doped CuCrO_2 target with limited and controlled oxygen loss during the deposition process and finally assists in the formation of the delafossite phase without (00 l) preferred orientation⁵² within the limit of the reduction of Cu(I) species into metallic copper nanoparticles.^{41,53} The expected stoichiometric oxygen content was independently supported by EPMA measurements carried out on silicon substrates whereas the cation (Cu + Cr + Mg) to anion (O) atomic ratio was found to be equal to 1 within the limit of the accuracy of the technique.

Microstructural analysis

The SEM image of the 300 nm as-deposited film in the cross-sectional view (Fig. 3a) reveals dense thin film with a very small particle size. An extremely low Root Mean Square (RMS) roughness estimated to be $\text{RMS} = 0.4 \text{ nm}$ is determined by AFM (Fig. 3b). This very weak surface topography is in good agreement with previous studies on delafossite materials deposited under the same (non-reactive magnetron sputtering of the oxide target)¹⁸ or similar (reactive magnetron sputtering of the metallic target)⁵⁴ deposition conditions. It also explains the impossibility of obtaining an exploitable SEM planar view even by the use of a field emission gun source. One can note that for a lower thickness

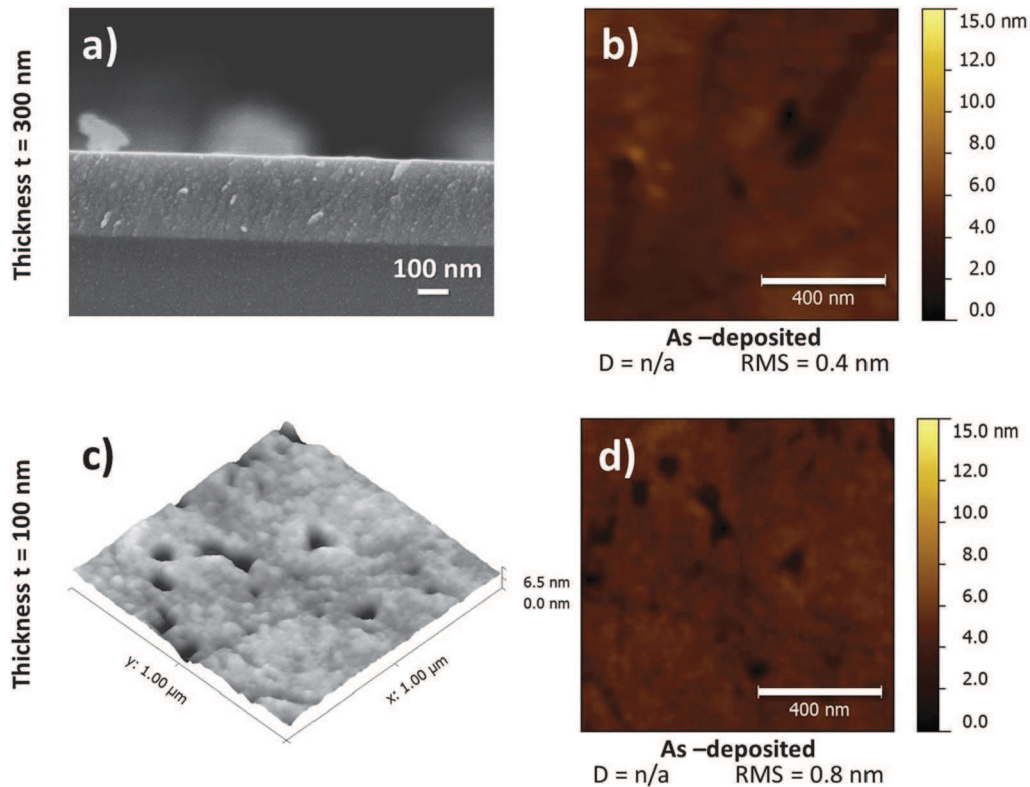


Fig. 3 (a) Cross section SEM and (b) surface AFM micrographs of 300 nm thick as-deposited thin film. The corresponding (c) 3D and (d) surface AFM micrographs of a 100 nm thick as-deposited film.

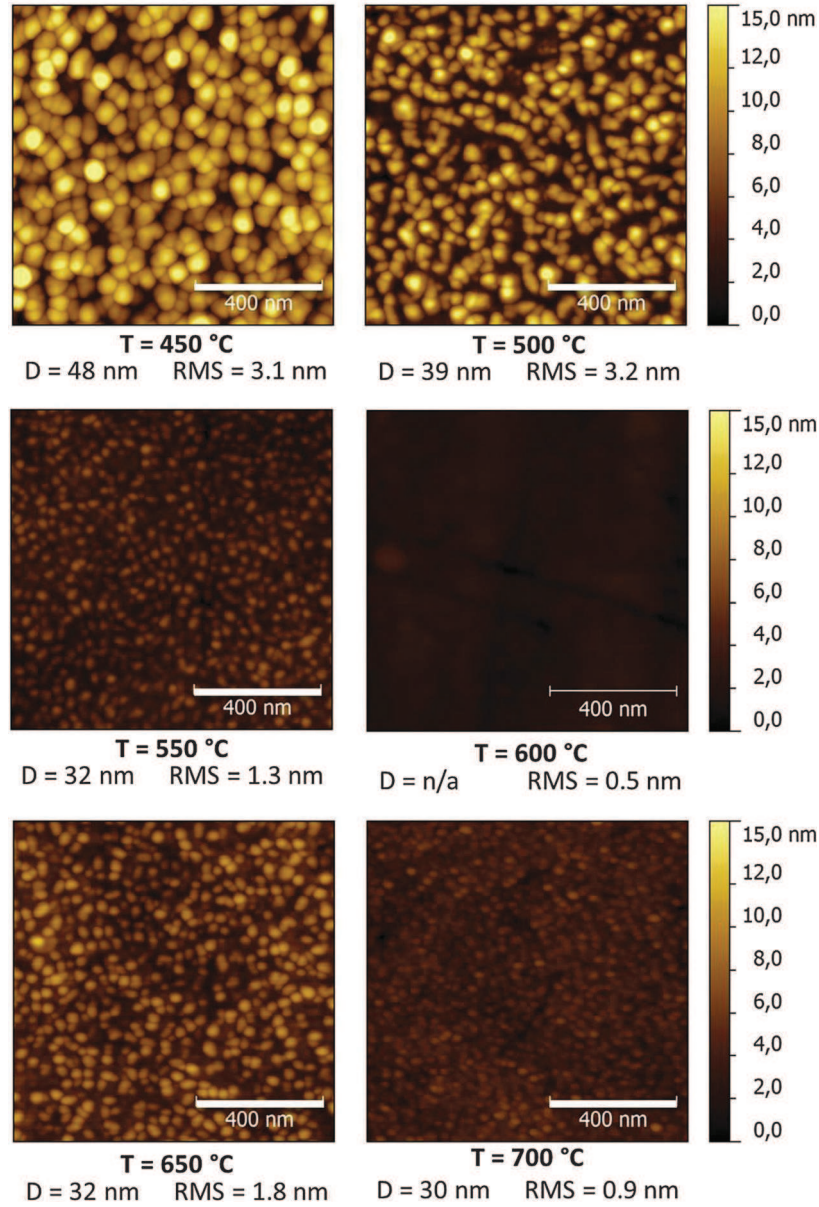


Fig. 4 AFM micrographs of 100 nm Mg-doped CuCrO₂ annealed at various temperatures in the range of 450 °C to 700 °C for 4 h under primary vacuum. The average particle size (D) and root mean square roughness (RMS) are indicated for all the samples.

of 100 nm, the as deposited film still presents a smooth surface with a very low roughness (RMS close to 0.8 nm) and a small grain size (Fig. 3c and d).

The AFM analysis of the Mg-doped CuCrO₂ thin films annealed at different temperatures reveals an important influence of the annealing temperature on the microstructure due to promotion of atom diffusion. For a film thickness of 100 nm, Fig. 4 shows the topographies obtained for different annealing temperatures in-between 450 and 700 °C.

In comparison with the pristine phase (100 nm as-deposited thin film shown in Fig. 3c and d), the 450 °C annealed thin film exhibits a well-defined grain shape with an average grain size of around 50 nm. From 450 to 600 °C, a constant decrease of the average grain size D and root mean square RMS clearly indicate

that crystallization and densification processes are in perfect agreement with the XRD analysis. At 600 °C which corresponds to the minimum temperature evidenced by TXRD analysis to obtain a characteristic splitting of the broad main diffraction peak into the (012) and (101) Bragg reflections of the Mg-doped CuCrO₂ phase, AFM shows a smooth surface with a minimum RMS value. Above 600 °C, small grains re-appear.

Even if the very weak surface roughness obtained for the as-deposited film is largely observed in many studies, the specific deposition conditions used in this work allows highlighting a particular microstructural evolution *versus* annealing temperature. Indeed, the normal growth of crystallites with temperature is followed by a reverse phenomenon leading to a decrease of size and the decay of the roughness, at about 600 °C. To a lesser extent,

this behavior was also observable in thin films deposited by reactive RF magnetron sputtering reported by Yu *et al.*⁵⁴

Four probe measurements

The transport properties of 100 nm and 300 nm thick as-deposited and annealed films were determined by in line four probe measurement at room temperature. The temperature dependence of the electrical conductivity σ for each compound is shown in Fig. 5a. The thickness dependence of electrical properties expressed in sheet resistance (R_s) is also plotted in Fig. 5b for film annealed at various temperatures.

Whatever the thickness is, the as-deposited Mg-doped CuCrO_2 thin films show an electrical conductivity σ lower than 0.0045 S cm^{-1} . This electrical conductivity increases with the annealing temperature especially from 450°C and reaches its maximum value $\sigma = 1.4 \text{ S cm}^{-1}$ at 600°C . For higher temperature, σ tends to decrease. For these temperatures, no increase in conductivity with the annealing time has been noticed. The optimal annealing temperature ($T = 600^\circ\text{C}$) corresponds to particular changes in the structural and microstructural behaviors: it is high enough to crystallize the delafossite phase but not too low to generate grain boundary resistivity. This result is consistent with the literature whereas some conductivities are reported for various annealing and/or deposition temperatures, for various deposition techniques and for various Mg-doping levels (RF-sputtered CuCrO_2 at T ,¹⁵ CuCrO_2 sol-gel processed and

post-annealed at T ,⁴⁵ chemical solution deposited $\text{CuCr}_{0.95}\text{Mg}_{0.05}\text{O}_2$ and post-annealed at T ,⁴⁸ pulsed laser deposited $\text{CuCr}_{0.92}\text{Mg}_{0.08}\text{O}_2$ at T ⁵⁵ and pulsed laser deposited $\text{CuCr}_{0.92}\text{Mg}_{0.08}\text{O}_2$ at T ⁵⁶). For comparison, values issued from these studies are reported in Fig. 5a.

The transport measurement proceeded as a function of the temperature under an air atmosphere, permits to determine the transport activation energy of all the annealed thin films. The transport activation energy decreases progressively until a stabilized value of 0.055 eV after a 600°C annealing process. The stabilized value has also been reported by Rastogi *et al.*⁵⁷ The activation energy is less than $3kT$ and justifies an important number of acceptor levels near the top of the valence band. This behavior corresponds to a highly doped degenerated semiconductor behavior. We noticed that this transport activation energy could increase from 55 meV at 250°C to 63 meV at 450°C under air then returns to 55 meV when the temperature drops to room temperature. This cycle generates also a permanent impact on the electrical conductivity which increases from 0.96 S cm^{-1} to 1.07 S cm^{-1} after the under air thermal cycle process. This behavior was explained by the intercalation of oxygen atoms into the copper plan of the delafossite structure according to the $(\text{Cu}^{+}_{1-x-2\delta}\text{Cu}^{2+}_{x+\delta})(\text{Fe}^{3+}_{1-x}\text{Mg}^{2+}_x)\text{O}_{2+\delta}$ formulae.

The electrical conductivity *versus* temperature in-between 150 and 400 K cannot be completely fitted by a classical thermal power law (adapted for classical semiconductors) in particular to the lower temperatures. Nevertheless, the $\sigma(T)$ curves can be fitted by the following two dimensional Mott relationship (eqn (1)):

$$\sigma(T) = A \cdot \exp\left(-\frac{T_{\text{Mott}}}{T}\right)^{1/n} \quad (1)$$

where σ is the material conductivity, A is an exponential pre-factor, T_{Mott} is the Mott temperature and $n = 3$ corresponds to the two dimensions transport. The $\sigma(T)$ behavior is in agreement with the hopping carrier mechanism.

Hall measurements

DC Hall measurements were processed on a 300 nm film annealed at 600°C for 4 h under vacuum and previously connected on a PPMS support by $20 \mu\text{m}$ aluminum wires thanks to Van der Pauw geometry. 3 T magnetic field and 0.05 mA current were applied to measure the electric potential. Nevertheless, no Hall effect has been measured using this DC technique with a moderate applied magnetic field. This supposes a too small carrier mobility and/or a too high carrier concentration which make sense with a hole concentration of about 10^{21} cm^{-3} reported by O'Sullivan *et al.*³⁴ on similar materials ($\text{CuCr}_{0.90}\text{Mg}_{0.10}\text{O}_2$) by AC Hall measurements using a magnetic field of 14 T .

Seebeck measurements

Fig. 6 shows the annealing temperature dependence of the Seebeck coefficient (S) measured at room temperature for the 100 nm thick Mg-doped CuCrO_2 films (300 nm thick films

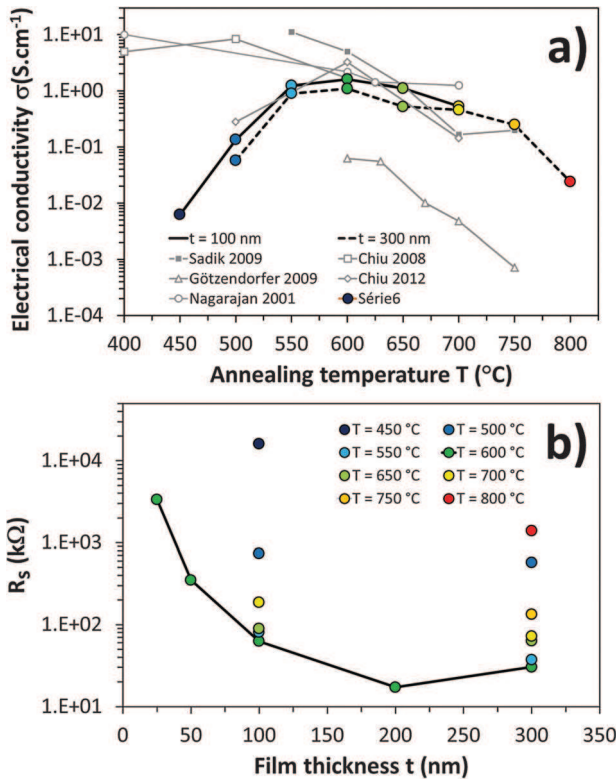


Fig. 5 (a) Electrical conductivity σ of the 100 nm and 300 nm thin films at different annealing temperatures. Some data from ref. 15, 25, 28, 35 and 36 are also plotted on this graph. (b) Sheet resistance $R_s = (\sigma \cdot \text{thickness})^{-1}$ as a function of the thickness for films annealed at various temperatures.

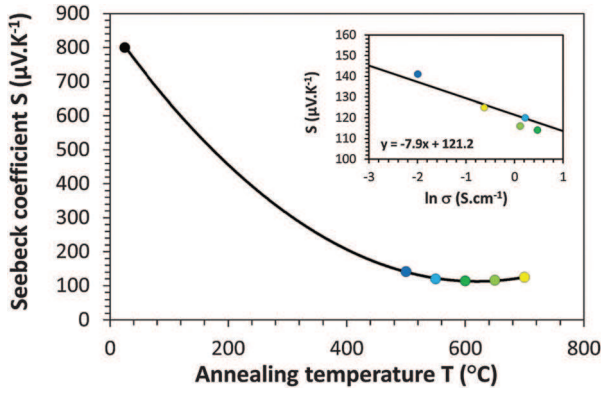


Fig. 6 The measured Seebeck coefficients (S) for 100 nm thick films annealed at different temperatures. Inset: Jonker's plot.

exhibit identical values and are not shown on this graph but are listed in Table 2). Whatever the thicknesses and the annealing temperatures are (including the as-deposited sample), S is positive. This indicates that the predominant charge carriers are positive holes, *i.e.* all the as-deposited and annealed Mg-doped CuCrO_2 films are p-type semiconductors.

The S value for the as-deposited sample is about $800 \mu\text{V K}^{-1}$. With the increase in annealing temperature up to 600°C , the S value drastically decreases down to about $110 \mu\text{V K}^{-1}$. For higher annealing temperatures ($T > 600^\circ\text{C}$), S slightly increases up to about $130 \mu\text{V K}^{-1}$. These Seebeck values are similar or lower than those reported in the literature for CuCrO_2 and Mg-doped CuCrO_2 due to the particular sensibility of S towards the Mg doping level and the thermal treatment.^{29,31,32,58} The evolution of S is in agreement with the evolution of the electrical conductivity: the lowest Seebeck coefficient is obtained for the highest electrical conductivity σ in agreement with Jonker's relationship.⁵⁹

In non-degenerate semiconductors, S and $\ln \sigma$ are reliable by an affine relationship. A plot of S versus $\ln \sigma$, called Jonker's plot, will have a slope of k_B/q ($-86.15 \mu\text{V K}^{-1}$ for p-type characteristics). In the case of the Mg-doped CuCrO_2 films, Jonker's plot (shown in the inset Fig. 6 for 100 nm thick samples) can be admittedly fitted with an affine relationship, but with a 10 times smaller slope. It then confirms that the carrier transport behavior does not follow a classical non-degenerate model and is

probably in favor of the hopping transport mechanism for degenerate semiconductors.

From the Seebeck coefficient measurement, it was possible to estimate the carrier concentration according to a Heikes formalism adapted for degenerate p-type semiconductors^{60–62} with a carrier hopping mechanism only in-between the $\text{Cu}^+/\text{Cu}^{2+}$ species present on the copper crystallographic site. In this case, the adapted Heikes formula is equal to eqn (2) as follows:

$$S = + \frac{k_B}{q} \ln \left[\left(\frac{g_1}{g_2} \right) \frac{[\text{Cu}^+]}{[\text{Cu}^{2+}]} \right] \quad (2)$$

where S is the experimental Seebeck coefficient (we suppose that S is saturated according to the Seebeck variation with the temperature mentioned in the literature for the 3% Mg-doped CuCrO_2 ⁴¹), k_B is the Boltzmann constant, q is the charge of the carrier, g_1 and g_2 are the electron degeneracy of Cu^+ and Cu^{2+} , respectively, and $[\text{Cu}^+]$ is the Cu^+ proportion ($[\text{Cu}^{2+}] = 1 - [\text{Cu}^+]$). The $3d^{10}$ Cu^+ ion shows a coordination number of two in the delafossite structure with a total spin of zero with only one orbital configuration. The electron degeneracy of Cu^+ is then equal to $g_1 = (2 \times 0 + 1) \times 1 = 1$. In the case of Cu^{2+} , the octahedral environment is preferred to the tetrahedral one,^{40,63} the electronic configuration is $3d^9$ and the spin is equal to $1/2$ with two orbital configurations. The electron degeneracy of Cu^{2+} is then equal to $g_2 = (2 \times 1/2 + 1) \times 2 = 4$.

Finally, for a $S = 114 \mu\text{V K}^{-1}$ obtained in the case of the 100 nm thick film annealed at 600°C , the proportion of Cu^+ is estimated to be 0.937 and consequently the complementary Cu^{2+} is 0.062 which corresponds to $x + \delta$ in the $(\text{Cu}_{1-x-2\delta}^{2+}\text{Cu}_{x+\delta}^{+})\text{O}_{2+\delta}$ formulae. This latest value makes sense with the Mg doping level ($x = 0.03$) and the very limited oxygen intercalation into the CuMO_2 delafossite with small M-cations such as Fe^{64} or Cr .⁴⁰ The density of the total copper sites in the delafossite structure is equal to $2.32 \times 10^{22} \text{ cm}^{-3}$ (site 3a (Fig. 1b) of the rhombohedral $R\bar{3}m$ space group in a hexagonal axis setup, and for a total unit cell volume $V = 129.36 \text{ \AA}^3$ determined by GIXRD). As each Cu^{2+} could generate a hole in the valence band, we can conclude that the hole density (determined from the S measurement) h_s is equal to $0.062 \times 2.32 \times 10^{22} = 1.45 \times 10^{21} \text{ cm}^{-3}$ under these conditions. The estimated carrier concentrations are exposed in Table 2 for every annealing temperature. They are once again in agreement

Table 2 Electrical (Seebeck coefficient S) and optical (TT and TR refined plasma frequency Ω_p and damping constant Ω_τ parameters) measurements and the corresponding carrier concentrations (h_{Elect} and h_{Opt}), mobility (μ_{Opt}) and the electrical conductivity (σ_{Opt}) of as-deposited and annealed 300 nm thick films

Annealing temperature, T ($^\circ\text{C}$)	Electrical measurements		Optical measurements				
	Seebeck coefficient, S ($\mu\text{V K}^{-1}$)	Carrier concentration, h_{Elect} (cm^{-3})	Plasma frequency, Ω_p (cm^{-1})	Damping constant, Ω_τ (cm^{-1})	Carrier concentration, h_{Opt} (cm^{-3})	Carrier mobility, μ_{Opt} ($\text{cm}^2 \text{ V}^{-1} \text{ s}^{-1}$)	Electrical conductivity, σ_{Opt} (S cm^{-1})
As-deposited	804	5.19×10^{17}	15	1475	6.30×10^{15}	2.530	0.002
500	140	1.09×10^{21}	7353	50 314	1.50×10^{21}	0.074	17.76
550	116	1.42×10^{21}	11 812	36 237	3.90×10^{21}	0.103	64.27
600	121	1.34×10^{21}	8741	24 055	2.13×10^{21}	0.155	52.82
650	122	1.32×10^{21}	6645	19 442	1.23×10^{21}	0.192	37.78
700	133	1.18×10^{21}	8597	22 950	2.00×10^{21}	0.163	52.16
750	167	8.07×10^{20}	4372	9137	5.30×10^{20}	0.408	34.60

with the AC Hall measurements³⁴ and the theoretical studies⁶⁵ exposed in the literature.

Optical properties

Optical spectra reported in Fig. 7 show the evolution of the integrated Total Transmittance (TT), Total Reflectance (TR) and calculated Total Absorbance ($TA = 1 - TT - TR$) in the 300 to 1100 nm wavelength range domain and for the 100 nm thick films annealed at different temperatures. The TT and TR spectra of thin films are highly reproducible for identical thickness and thermal treatment.

The TT spectra show an increase of the average integrated total transmittance $\langle TT \rangle$ in the 400 to 800 nm visible range from 46% to 69% when the annealing temperature increases from 450 to 800 °C, respectively (inset of Fig. 7a). Any notable variation of the reflectance is observed (Fig. 7b). The optical bandgap has been calculated by the direct band gap of Tauc's relationship⁶⁶ employed from the integrated transmittance data. The optical bandgap increases with the annealing temperature until a maximum value of $E_g = 3.3$ eV as shown in the inset of Fig. 7c. This maximal E_g value corresponds to the stabilized structure gap energy obtained for the optimal annealing temperature (600 °C) in good agreement with the previous structural and microstructural analyses. $E_g = 3.3$ eV obtained for Mg-doped CuCrO_2 films is just larger than those reported in the literature for various un-doped CuCrO_2 phases (from 3.05 to 3.20 eV depending on the deposition technique and thermal treatment^{47,49–51,58,67}). This slight increase of the gap energy is correlated with the slight increase of acceptor levels in the forbidden band according to the Burnstein–Moss effect.⁶⁸ It is consistent with the Mg insertion in the delafossite structure as already reported in the literature.^{19,56}

Opto-electrical properties

TT and TR spectra were fitted simultaneously using the SCOUT software⁴³ thank to dielectric models, which integrate a Kramer Kronig relationship for interband transition⁶⁹ and Drude and Kim oscillators.⁷⁰ The Kramer Kronig relationship model incorporates a strength oscillator and the gap energy (which is approached by the experimental data obtained from the spectra). A Kim oscillator integrates the resonance frequency, oscillator strength and damping parameters. From the Drude model, the dielectric carrier contribution is calculated from the plasma frequency and the carrier damping parameter. The total film thickness is initially set to the experimental value determined by mechanical profilometry and confirmed by X-ray reflectometry.

The refinement of these seven adjustable parameters (strength oscillator, gap energy, resonance frequency, oscillator strength, damping, plasma frequency and carrier damping) as well as the adjustment of the total thickness permits us to obtain a good fit of the experimental TT and TR spectra simultaneously. The satisfactory refinement of the dielectric model from optical data was initially obtained on the thicker film (≈ 300 nm) and validated just by thickness adjustment on the thinner one (≈ 300 nm). An example of TT and TR fits for

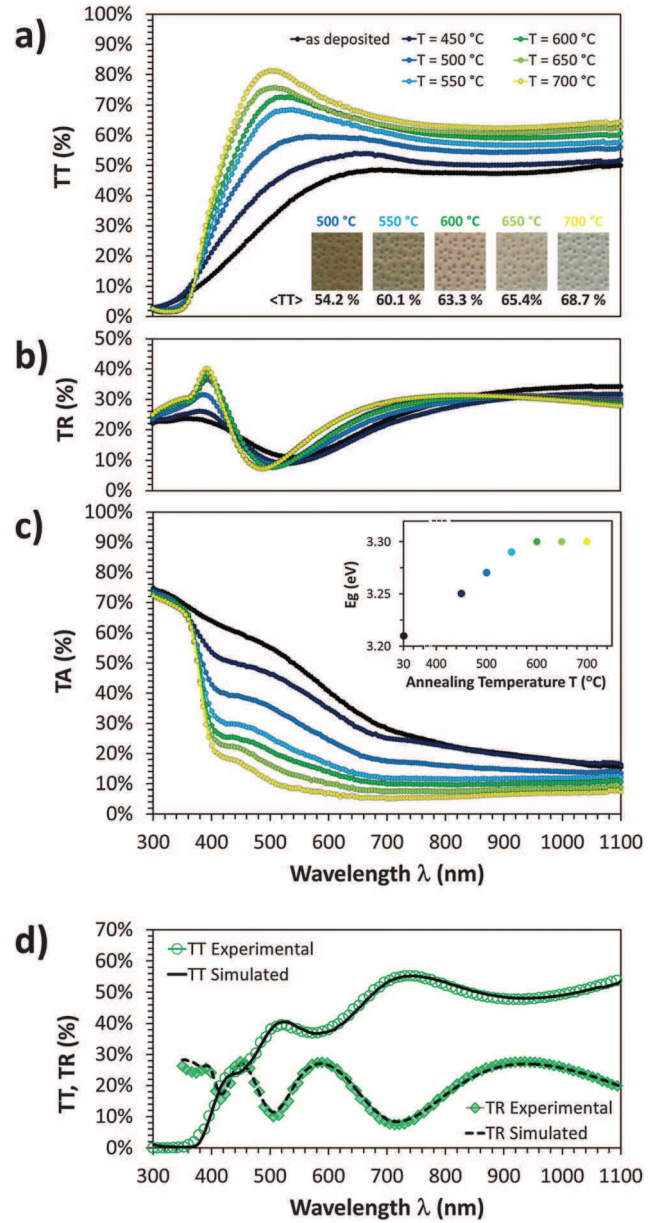


Fig. 7 (a) TT (b) TR and (c) TA optical spectra of 100 nm thin films deposited on a quartz substrate and annealed at different temperatures. Pictures of these films treated at different temperatures and placed on a medium of patterned paper, are presented in inset (a) to illustrate their transparency to natural white light. Values of the average total transmittance $\langle TT \rangle$ of the films in the 400 to 800 nm visible range are also reported as a function of the annealing temperature in inset (a). The direct optical bandgap calculated from Tauc's relationship as a function of the annealing temperature is plotted in inset (c). (d) TT and TR optical spectra of a 300 nm thin film and the corresponding simulated TT and TR spectra.

the 300 nm Mg-doped CuCrO_2 film annealed at 600 °C is reported in Fig. 7d. The standard deviation of the TT and TR spectra simultaneously fit is less than 4.4×10^{-4} (1.2×10^{-4} for TT and 3.2×10^{-4} for TR, respectively).

Within these optical measurements, the hole density (n_{opt}) and carrier mobility (μ_{opt}) and then the corresponding equivalent conductivity (σ_{opt}) can be deduced from the refined plasma

frequency (Ω_p) and carrier damping (Ω_τ) parameters according to eqn (3) and (4), respectively, as follows:

$$h_{\text{Opt}} = \frac{4\pi^2 c^2 \varepsilon_0 m^*}{q^2} \Omega_p^2 \quad (3)$$

$$\mu_{\text{Opt}} = \frac{q}{2\pi c m^* \Omega_\tau} \quad (4)$$

where c is the speed of light, ε_0 the vacuum permittivity, q the charge of the carrier and m^* the hole effective mass. $m^* = 2.5 m_e$ found in the literature⁷¹ has been used. In addition to the electrical data, the refinement of optical data (Ω_p and Ω_τ) and deduced (h_{Opt} , μ_{Opt} and σ_{Opt}) parameters are reported in Table 2 for the 300 nm thick film at different annealing temperatures.

The electrical characteristics deduced from the optical simulation show slightly higher carrier concentrations (h_{Opt}) than those estimated in this work by Seebeck measurements (h_{Elect}) and in the literature by AC Hall measurements.³⁴ One can note that such a high carrier concentration h_{Opt} of about 10^{21} cm^{-3} has already been reported by Obulapathi *et al.*⁷² on similar CuCrO₂ films. A lower value of the carrier concentration determined by Seebeck measurements (h_{Elect}) than those estimated by optical data (h_{Opt}) and then a lower measured conductivity than σ_{Opt} could be due to the trapping of some carriers in the various defects as grain boundaries and/or surface traps. All the annealed samples also exhibit a very low mobility ($\mu_{\text{Opt}} < 0.4 \text{ cm}^2 \text{ V}^{-1} \text{ s}^{-1}$) in good accordance with the strongly correlated system (hopping mechanism) and previous reports.¹⁵

All the electrical characteristics (S , h_{Elect} , h_{Opt} , σ , σ_{Opt}) evolve in the same way and exhibit an optimal value for the 600 °C annealing sample. This 600 °C annealed sample is still the most optimized p-type TCO sample with a maximum value of figure of merit (FOM), which also takes into account the optical properties. For the 600 °C annealing sample, FOM reaches $1.5 \times 10^{-7} \Omega^{-1}$ according to $\text{FOM} = \langle \text{TT} \rangle^{10} / R_s$ defined by Haacke⁷³ where R_s (Ω) is the sheet resistance of the film and $\langle \text{TT} \rangle$ is the average total transmittance of the film in the 400 to 800 nm range. This FOM value is higher than $\text{FOM} = 3.2 \times 10^{-8} \Omega^{-1}$ and $\text{FOM} = 4.2 \times 10^{-8} \Omega^{-1}$ obtained for instance by Nagarajan *et al.*¹⁵ ($\sigma = 220 \text{ S cm}^{-1}$ and $\langle \text{TT} \rangle = 30\%$ for a 250 nm thick film of CuCr_{0.95}Mg_{0.05}O₂) and Li *et al.*⁷⁴ ($\sigma = 0.33 \text{ S cm}^{-1}$ and $\langle \text{TT} \rangle = 63\%$ for a 127 nm thick film of CuCrO₂).

Optical index

Although the refractive index n is one of the most basic optical properties, to our knowledge its determination has never been reported for Mg-doped CuCrO₂ materials. More generally, only a few determinations of delafossite have been reported so far^{75,76} and often derived from reflectivity measurements.^{74,77} Here, the Mg-doped CuCrO₂ complex index of refraction (n , k) were measured by spectroscopic ellipsometry (SE) and compared to those determined from the refinement of the optical data and those obtained using the envelop methods.⁷⁸ For the determination of the complex index of refraction (n and k) by ellipsometry, the data were fitted with a model consisting of three layers: a quartz substrate, the delafossite film, and a surface

roughness layer. The latter was modeled with a layer constituted of a mixture of 50% Mg-doped CuCrO₂ and 50% void according to the Bruggeman effective medium approximation (BEMA).⁷⁹ Fig. 8a shows the fitting of ellipsometric data, I_s ($\sin 2\Psi \times \sin \Delta$) and I_c ($\sin 2\Psi \times \cos \Delta$) modeled using Tauc-Lorentz dispersion relationships⁸⁰ for the 300 nm thick Mg-doped CuCrO₂ film annealed at 600 °C. The goodness of the fit can be estimated by the value of the mean square error value χ^2 . In our case a low value of χ^2 has been obtained ($\chi^2 = 2.93$). The fitting results indicated that the thickness of the film was $286.7 \pm 0.9 \text{ nm}$ and that the surface roughness layer was $6.8 \pm 0.2 \text{ nm}$, *i.e.* a total thickness of $293.5 \pm 1.1 \text{ nm}$ in agreement with the previous measurements done by profilometry and X-ray reflectometry. The evolution of n and k in the range 350–1000 nm, which have been deduced from the ellipsometric model, is presented in Fig. 8b. The value of $n \approx 2.4$ at 1000 nm in wavelength can be put forward, which is quite similar to those obtained at a wavelength of 1100 nm on a CuAlO₂ single crystal ($n = 2.32$) and CuInO₂ ($n = 2.1$) by optical methods^{75,76} and *ab initio* calculations.⁸¹ In contrast, this value is really different from $n = 1.2$ at 650 nm announced by Li *et al.*⁷⁴ for CuCrO₂ which seems to be unrealistic given the delafossite electronic structure.

The refinement of the dielectric model from optical data was also used to determine the material susceptibility and then

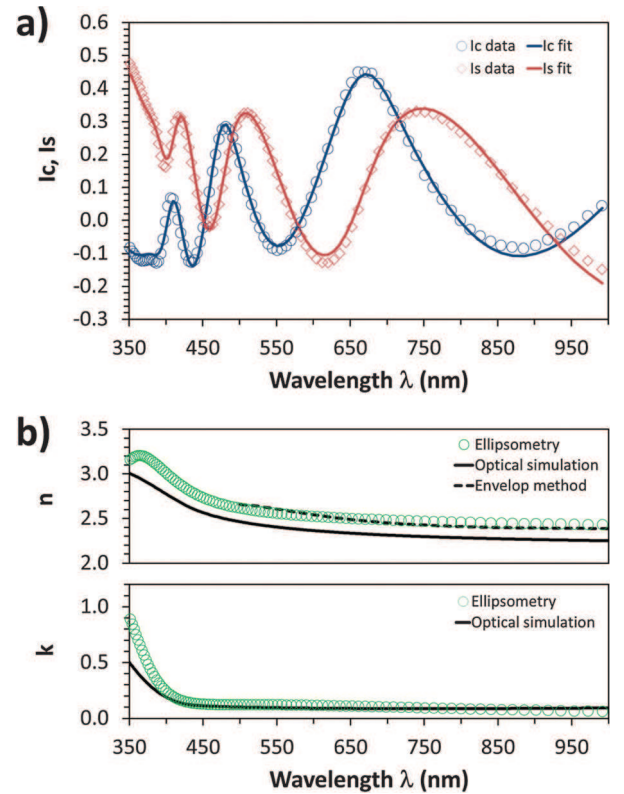


Fig. 8 300 nm thick Mg-doped CuCrO₂ film annealed at 600 °C optical constants. (a) Experimental and simulated ellipsometric data I_s ($\sin 2\Psi \times \sin \Delta$) and I_c ($\sin 2\Psi \times \cos \Delta$) as a function of optical wavelength, and (b) the corresponding optical constants, n and k , determined from analysis of ellipsometry data (green circles), and TT and TR data (refinement of the dielectric model is indicated by the black full line and the envelop method is indicated by the dashed line).

permits us to calculate the complex index of refraction (n , k) as a function of the wavelength. Fig. 8b compares the optical constants (n , k) determined by ellipsometry, refinement of the optical data and the envelop methods. Even if the complementary values of n estimated by spectrophotometry are slightly below those deduced from SE data due to the use of different techniques and models, these optical refractive index values remains however in the same range.

4. Conclusions

This work provides an insight into the delafossite Mg-doped CuCrO₂ thin film deposition and opto-electronic properties. It offers complete structural, microstructural, electrical and optical characterization helpful for the understanding and optimization of technologically relevant p-type TCO materials.

The Mg-doped CuCrO₂ thin films were deposited on a quartz substrate by magnetron sputtering using a homemade ceramic target, and then annealed at various temperatures for 4 h under vacuum in the 450 to 800 °C range. The structural characterization shows an increase in the delafossite crystallinity with the annealing temperature. The limited and controlled oxygen loss during the deposition and annealing processes assists in the formation of the delafossite phase without any particular (00 l) preferred orientation within the limit of the reduction of Cu(I) species into metallic copper nanoparticles.

The microstructural analysis emphasizes a very weak surface roughness for the as-deposited film and highlights a particular microstructural evolution *versus* annealed temperature with a rupture in crystallite growth at about 600 °C. This temperature was considered as the optimal temperature for the study of p-type TCO properties.

Different characterization methods were used to determine the carrier concentration in Mg-doped CuCrO₂ thin films. The DC Hall measurement has not permitted us to estimate a carrier density, whereas the Seebeck measurement allows us to justify the positive holes as predominant charge carriers and estimate the effective carrier concentration of about 10²¹ cm⁻³ with the hopping transport formalism. Measurements of transmittance and reflectance associated with a dielectric model corroborated these values. These optical measurements also allowed us to determine for the first time the refractive index (n , k) of Mg-doped CuCrO₂. A value of $n = 2.3$ at 1100 nm was obtained, which is close to those of most of other copper delafossites. Spectroscopic ellipsometry confirmed the order of magnitude of the refractive index and the extinction coefficient deduced from the transmittance and reflectance spectra. The optimal TCO properties of the Mg-doped CuCrO₂ thin films of 100 nm thickness after a 600 °C annealing for 4 h under vacuum treatment are obtained. It shows an electrical conductivity of $\sigma = 1.4$ S cm⁻¹ and an average transmittance of 63% in the visible range. Haacke's figure of merit of these Mg-doped CuCrO₂ thin films is equal to 1.5×10^{-7} Ω^{-1} . This result is one of the best FOM value reported to date for the p-type TCO material. Moreover, it was obtained for films processed at

moderate temperature. Accordingly, RF-sputtered Mg-doped CuCrO₂ thin films show promising results for future transparent electronic device conception.

Acknowledgements

The authors gratefully acknowledge the support from Institut Carnot CIRIMAT (bourse de these Carnot M. Lalanne), the Fédération de Recherche FERMAT (temperature XRD and PVE measurements) and the French RENATECH network through Institut Carnot LAAS (ellipsometry measurements).

References

- 1 A. Stadler, Transparent Conducting Oxides - An up-to-date overview, *Materials*, 2012, **5**, 661–683.
- 2 L. Castaneda, Present status of the development and application of Transparent Conductors Oxide thin solid films, *Mater. Sci. Appl.*, 2011, **2**, 1233–1242.
- 3 D. S. Ginley and C. Bright, Transparent conducting oxides, *MRS Bull.*, 2000, **8**, 15–18.
- 4 H. Kawazoe, M. Yasukawa, H. Hyodo, M. Kurita, H. Yanagi and H. Hosono, P-type electrical conduction in transparent thin films of CuAlO₂, *Nature*, 1997, **389**, 939–942.
- 5 R. Seshadri, C. Felser, K. Thiem and W. Tremel, Metal-metal bonding and metallic behavior in some ABO₂ delafossites, *Chem. Mater.*, 1998, **10**, 2189–2196.
- 6 H. Yanagi, S. Park, A. Draeseke, D. Keszler and J. Tate, P-type conductivity in transparent oxides and sulfide fluorides, *J. Solid State Chem.*, 2003, **175**, 34–38.
- 7 A. N. Banerjee and K. K. Chattopadhyay, Recent developments in the emerging field of crystalline p-type transparent conducting oxide thin films, *Prog. Cryst. Growth Charact. Mater.*, 2005, **50**, 52–105.
- 8 S. Sheng, G. Fang, C. Li, S. Xu and X. Zhao, P-type transparent conducting oxides, *Phys. Status Solidi A*, 2006, **203**, 1891–1900.
- 9 B. Ingram, G. Gonzalez, T. Mason, D. Shahriari, A. Barnabé, D. Ko and P. Poepelmeier, Transport and defect mechanisms in cuprous delafossites. 1. Comparison of hydrothermal and standard solid-state synthesis in CuAlO₂, *Chem. Mater.*, 2004, **16**, 5616–5622.
- 10 H. Kawazoe, H. Yanagi, K. Ueda and H. Hosono, Transparent p-type conducting oxides: design and fabrication of p-n heterojunctions, *Mater. Res. Soc. Bull.*, 2000, **8**, 28–36.
- 11 J. Tate, M. Jayaraj, A. Draeseke, T. Ulbrich, A. Sleight, K. Vanaja, R. Nagarajan, J. Wager and R. Hoffman, P-Type oxides for use in transparent diodes, *Thin Solid Films*, 2002, **411**, 119–124.
- 12 H. Yanagi, T. Hase, S. Ibuki, K. Ueda and H. Hosono, Bipolarity in electrical conduction of transparent oxide semiconductor CuInO₂ with delafossite structure, *Appl. Phys. Lett.*, 2001, **78**, 1583–1585.
- 13 M. Jayaraj, A. Draeseke, J. Tate and A. Sleight, P-Type transparent thin films of CuY_{1-x}Ca_xO₂, *Thin Solid Films*, 2001, **397**, 244–248.

- 14 Y. Takehi, K. Satoh, T. Yotsuya, A. Ashida, T. Yoshimura and N. Fujimura, Electrical and optical properties of excess oxygen intercalated $\text{CuScO}_2(0001)$ epitaxial films prepared by oxygen radical annealing, *Thin Solid Films*, 2008, **516**, 5785–5789.
- 15 R. Nagarajan, A. Draeseke, A. Sleight and J. Tate, P-type conductivity in $\text{CuCr}_{1-x}\text{Mg}_x\text{O}_2$ films and powders, *J. Appl. Phys.*, 2001, **89**, 8022–8025.
- 16 G. Thomas, Invisible circuits, *Nature*, 1997, **389**, 907–908.
- 17 J. Wager, D. Kesler and D. Presley, *Transparent Electronics*, Springer edn, 2008.
- 18 A. Barnabé, E. Mugnier, L. Presmanes and P. Tailhades, Preparation of delafossite CuFeO_2 thin films by rf-sputtering on conventional glass substrate, *Mater. Lett.*, 2006, **60**, 3468–3470.
- 19 X. Li, M. Han, X. Zhang, C. Shan, Z. Hu, Z. Zhu and J. Chu, Temperature-dependent band gap, interband transitions, and exciton formation in transparent p-type delafossite $\text{CuCr}_{1-x}\text{Mg}_x\text{O}_2$ films, *Phys. Rev. B: Condens. Matter Mater. Phys.*, 2014, **90**, 035308.
- 20 T. Chiu, Y. Yang, A. Yeh, Y. Wang and Y. Feng, Antibacterial property of CuCrO_2 thin films prepared by RF magnetron sputtering deposition, *Vacuum*, 2013, **87**, 174–177.
- 21 R. Rao, A. Dandekar, R. Baker and M. Vannice, Properties of copper chromite catalysts in hydrogenation reactions, *J. Catal.*, 1997, **171**, 406–419.
- 22 A. Amrute, G. Larrazábal, C. Mondelli and J. Pérez-Ramírez, CuCrO_2 Delafossite: a stable copper catalyst for chlorine production, *Angew. Chem.*, 2013, **52**, 9772–9775.
- 23 P. Zhang, Y. Shi, M. Chi, J. Park, G. Stucky, E. McFarland and L. Gao, Mesoporous delafossite CuCrO_2 and spinel CuCr_2O_4 : synthesis and catalysis, *Nanotechnology*, 2013, **24**, 345704.
- 24 S. Saadi, A. Bouguelia and M. Trari, Photocatalytic hydrogen evolution over CuCrO_2 , *Sol. Energy*, 2006, **80**, 272–280.
- 25 T. Okuda, T. Onoe, Y. Beppu, N. Terada, T. Doi, S. Miyasaka and Y. Tokura, Magnetic and transport properties of delafossite oxides $\text{CuCr}_{1-x}(\text{Mg,Ca})_x\text{O}_2$, *J. Magn. Magn. Mater.*, 2007, **310**, 890–892.
- 26 A. Maignan, C. Martin, R. Frésard, V. Eyert, E. Guilmeau, S. Hébert, M. Poienar and D. Pelloquin, On the strong impact of doping in the triangular antiferromagnet CuCrO_2 , *Solid State Commun.*, 2009, **149**, 962–967.
- 27 M. Poienar, F. Damay, C. Martin, V. Hardy, A. Maignan and G. Andre, Structural and magnetic properties of $\text{CuCr}_{1-x}\text{Mg}_x\text{O}_2$ by neutron powder diffraction, *Phys. Rev. B: Condens. Matter Mater. Phys.*, 2009, **79**, 014412.
- 28 T. Okuda, N. Jufuku, S. Hidaka and N. Terada, Magnetic, transport, and thermoelectric properties of the delafossite oxides $\text{CuCr}_{1-x}\text{Mg}_x\text{O}_2$ ($0 \leq x \leq 0.04$), *Phys. Rev. B: Condens. Matter Mater. Phys.*, 2005, **72**, 144403.
- 29 Y. Ono, K. Satoh, T. Nozaki and T. Kajitani, Structural, magnetic and thermoelectric properties of delafossite-type oxide; $\text{CuCr}_{1-x}\text{Mg}_x\text{O}_2$ ($0 \leq x \leq 0.05$), *Jpn. J. Appl. Phys.*, 2007, **46**, 1071–1075.
- 30 K. Hayashi, K. Sato, K. Nozaki and T. Kajitani, Effect of doping on thermoelectric properties of delafossite-type Oxide CuCrO_2 , *Jpn. J. Appl. Phys.*, 2008, **57**, 59–63.
- 31 E. Guilmeau, M. Poienar, S. Kremer, S. Marinell, S. Hébert, R. Frésard and A. Maignan, Mg Substitution in CuCrO_2 delafossite compounds, *Solid State Commun.*, 2011, **23**, 1798.
- 32 Q. Meng, S. Lu, S. Lu and Y. Xiang, Preparation of p-type $\text{CuCr}_{1-x}\text{Mg}_x\text{O}_2$ bulk with improved thermoelectric properties by sol-gel method, *J. Sol-gel Sci. Technol.*, 2012, **63**, 1–7.
- 33 M. Soda, K. Kimura, T. Kimura and K. Hirota, Domain rearrangement and spin-spiral-plane flop as sources of magnetoelectric effects in delafossite CuCrO_2 , *Phys. Rev. B: Condens. Matter Mater. Phys.*, 2010, **81**, 100406.
- 34 M. O'Sullivan, P. Stamenov, J. Alaria, M. Venkatesan and J. M. D. Coey, Magnetoresistance of CuCrO_2 -based delafossite films, *J. Phys.: Conf. Ser.*, 2010, **200**, 052021.
- 35 S. Zhou, X. Fang, Z. Deng, D. Li, W. Dong, R. Tao, G. Meng and T. Wang, Room temperature ozone sensing properties of p-type CuCrO_2 nanocrystals, *Sens. Actuators, B*, 2009, **143**, 119–123.
- 36 D. Xiong, Z. Xu, X. Zeng, W. Zhang, W. Chen, X. Xu, M. Wang and Y. Cheng, Hydrothermal synthesis of ultra-small CuCrO_2 nanocrystal alternatives to NiO nanoparticles in efficient p-type dye-sensitized solar cells, *J. Mater. Chem.*, 2012, **22**, 24760–24768.
- 37 J. Shu, X. Zhu and T. Yi, CuCrO_2 as anode material for lithium ion batteries, *Electrochim. Acta*, 2009, **54**, 2795–2799.
- 38 M. J. Han, Z. H. Duan, J. Z. Zhang, S. Zhang, Y. W. Li, Z. G. Hu and J. H. Chu, Electronic transition and electrical transport properties of delafossite $\text{CuCr}_{1-x}\text{Mg}_x\text{O}_2$ ($0 \leq x \leq 12\%$) films prepared by the sol-gel method: A composition dependence study, *J. Appl. Phys.*, 2013, **114**, 163526.
- 39 M. Lalanne, M. Demont and A. Barnabé, AC conductivity and dielectric properties of $\text{CuFe}_{1-x}\text{Cr}_x\text{O}_2$:Mg delafossite, *J. Phys. D: Appl. Phys.*, 2011, **44**, 185401.
- 40 M. Lalanne, A. Barnabé, F. Mathieu and P. Tailhades, Synthesis and thermostructural studies of a $\text{CuFe}_{1-x}\text{Cr}_x\text{O}_2$ Delafossite solid solution with $0 \leq x \leq 1$, *Inorg. Chem.*, 2009, **48**, 6065–6071.
- 41 E. Mugnier, A. Barnabé, L. Presmanes and P. Tailhades, Thin films preparation by rf-sputtering of copper/iron ceramic targets with $\text{Cu/Fe} = 1$: From nanocomposites to delafossite compounds, *Thin Solid Films*, 2008, **516**, 1453–1456.
- 42 D. Necas, P. Klapetek, Gwyddion data analysis software. <http://gwyddion.net/>.
- 43 W. Theiss; Hard & Software. <http://www.mtheiss.com/>.
- 44 K. Tonooka and N. Kikuchi, Preparation of transparent CuCrO_2 :Mg/ZnO p-n junctions by pulsed laser deposition, *Thin Solid Films*, 2006, **515**, 2415–2418.
- 45 S. Götzendörfer, C. Polenzky, S. Ulrich and P. Löbmann, Preparation of p-type conducting transparent CuCrO_2 and $\text{CuAl}_{0.5}\text{Cr}_{0.5}\text{O}_2$ thin films by sol-gel processing, *J. Sol-Gel Sci. Technol.*, 2009, **52**, 113–119.
- 46 R. Bywalez, S. Götzendörfer and P. Löbmann, Structural and physical effects of Mg-doping on p-type CuCrO_2 and

- CuAl_{0.5}Cr_{0.5}O₂ thin films, *J. Mater. Chem.*, 2010, **20**, 6562–6570.
- 47 H. Chen, W. Yang and K. Chang, Characterization of delafossite-CuCrO₂ thin films prepared by post-annealing using an atmospheric pressure plasma torch, *Appl. Surf. Sci.*, 2012, **258**, 8775–8779.
 - 48 T. Chiu, S. Tsai, Y. Wang and K. Hsu, Preparation of p-type conductive transparent CuCrO₂:Mg thin films by chemical solution deposition with two-step annealing, *Ceram. Int.*, 2012, **48**, S673–S676.
 - 49 D. Li, X. Fang, A. Zhao, Z. Deng, W. Dong and T. Tao, Physical properties of CuCrO₂ films prepared by pulsed laser deposition, *Vacuum*, 2010, **84**, 851–856.
 - 50 S. Mahapatra and S. Shivashankar, Low-pressure metal-organic CVD of transparent and p-type conducting CuCrO₂ thin films with high conductivity, *Chem. Vap. Deposition*, 2003, **9**, 238–240.
 - 51 G. Dong, M. Zhang, X. Zhao, H. Yan, C. Tian and Y. Ren, Improving the electrical conductivity of CuCrO₂ thin film by N doping, *Appl. Surf. Sci.*, 2010, **256**, 4121–4124.
 - 52 V. Varadarajan and D. P. Norton, CuGaO₂ thin film synthesis using hydrogen-assisted pulsed laser deposition, *Appl. Phys. A: Mater. Sci. Process.*, 2006, **85**, 117–120.
 - 53 A. Barnabé, A. Chapelle, L. Presmanes and P. Tailhades, Copper and iron based thin film nanocomposites prepared by radio frequency sputtering. Part I: elaboration and characterization of metal/oxide thin film nanocomposites using controlled *in situ* reduction process, *J. Mater. Sci.*, 2013, **48**, 3386–3394.
 - 54 R. S. Yu and C. M. Wu, Characteristics of p-type transparent conductive CuCrO₂ thin films, *Appl. Surf. Sci.*, 2013, **282**, 92–97.
 - 55 T. Chiu, K. Tonooka and N. Kikuchi, Fabrication of ZnO and CuCrO₂: Mg thin films by pulsed laser deposition with *in situ* laser annealing and its application to oxide diodes, *Thin Solid Films*, 2008, **516**, 5941–5947.
 - 56 P. Sadik, M. Ivill, V. Craciun and D. Norton, Electrical transport and structural study of CuCr_{1-x}Mg_xO₂ delafossite thin films grown by pulsed laser deposition, *Thin Solid Films*, 2009, **517**, 3211–3215.
 - 57 A. C. Rastogi, S. H. Lim and S. B. Desu, Structure and optoelectronic properties of spray deposited Mg doped p-CuCrO₂ semiconductor oxide thin films, *J. Appl. Phys.*, 2008, **104**, 023712.
 - 58 R. Nagarajan, N. Duan, M. Jayaraj, J. Li, K. Vanaja, A. Yokochi, A. Draeseke, J. Tate and A. Sleight, P-type conductivity in the delafossite structure, *Int. J. Inorg. Mater.*, 2001, **3**, 265–270.
 - 59 G. Jonker, The application of combined conductivity and Seebeck-effect plots for the analysis of semiconductor properties, *Philips Res. Rep.*, 1968, **23**, 131–138.
 - 60 R. R. Heikes and R. W. Ure, Thermoelectricity: Science and Engineering, *Interscience*, 1961, **81**, DOI: 10.1016/0011-2275(62)90062-0.
 - 61 W. Ketir, S. Saadi and M. Trari, Physical and photoelectrochemical characterization of CuCrO₂ single crystal, *J. Solid State Electrochem.*, 2012, **16**, 213–218.
 - 62 W. Koayashi, I. Terasaki, M. Mikami and R. Funahashi, Negative Thermoelectric Power Induced by Positive Carriers in CaMn_{3-x}Cu_xMn₄O₁₂, *J. Phys. Soc. Jpn.*, 2004, **73**, 523–525.
 - 63 A. Navrotsky and O. J. Kleppa, The thermodynamics of cation distributions in simple spinels, *J. Inorg. Nucl. Chem.*, 1967, **29**, 2701.
 - 64 E. Mugnier, A. Barnabé and P. Tailhades, Synthesis and characterization of CuFeO_{2+δ} delafossite powders, *Solid State Ionics*, 2006, **177**, 607–612.
 - 65 D. Scanlon, A. Walsh and G. W. Watson, Understanding the p-type conduction properties of the transparent conducting oxide CuBO₂: A Density Functional Theory Analysis, *Chem. Mater.*, 2009, **21**, 4568–4576.
 - 66 J. Tauc, Optical properties and electronic structure of amorphous Ge and Si, *Mater. Res. Bull.*, 1968, **3**, 37–46.
 - 67 D. Shin, J. Foord, R. Egdell and A. Walsh, Electronic structure of CuCrO₂ thin films grown on Al₂O₃(001) by oxygen plasma assisted molecular beam epitaxy, *J. Appl. Phys.*, 2012, **112**, 113718.
 - 68 E. Burnstein, Anomalous optical absorption limit in InSb, *Phys. Rev.*, 1954, **93**(3), 632–633.
 - 69 F. Demichelis, G. Kaniadakis, A. Tagliaferro and E. Tresso, New approach to optical analysis of absorbing thin solid films, *Appl. Opt.*, 1987, **26**, 1737.
 - 70 C. C. Kim, J. W. Garland, H. Abad and P. M. Raccach, Modeling the optical dielectric function of semiconductors: extension of the critical-point parabolic-band approximation, *Phys. Rev. B: Condens. Matter Mater. Phys.*, 1992, **45**, 11749.
 - 71 G. Hautier, A. Miglio, G. Ceder, G.-M. Rignanese and X. Gonze, Identification and design principles of low hole effective mass p-type transparent conducting oxides, *Nat. Commun.*, 2013, **4**, 2292.
 - 72 L. Obulapathi, A. GuruSampath Kumar, T. Sofi Saramash, D. Jhansi Rani and T. Subba Rao, Effect of Annealing temperature on structural, electrical and optical properties of CuCrO₂ thin films by reactive DC magnetron sputtering, *Int. J. Res. Pure Appl. Phys.*, 2014, **4**, 16–19.
 - 73 G. Haacke, New figure of merit for transparent conductors, *J. Appl. Phys.*, 1976, **47**, 4086E9.
 - 74 D. Li, X. Fang, A. Zhao, Z. Deng, W. Dong and R. Tao, Physical properties of CuCrO₂ films prepared by pulsed laser deposition, *Vacuum*, 2010, **84**, 851–856.
 - 75 J. Pellicer-Porres, A. Segura and D. Kim, Refractive index of the CuAlO₂ delafossite, *Semicond. Sci. Technol.*, 2009, **24**, 015002.
 - 76 C. Teplin, T. Kaydanova, D. Young, J. Perkins, D. Ginley, A. Ode and D. Readey, A simple method for the preparation of transparent p-type Ca-doped CuInO₂ films: Pulsed-laser deposition from air-sintered Ca-doped Cu₂In₂O₅ targets, *Appl. Phys. Lett.*, 2004, **85**, 3789–3791.
 - 77 A. Banerjee, C. Ghosh, S. Das and K. Chattopadhyay, Electro-optical characteristics and field-emission properties of reactive DC-sputtered p-CuAlO_{2+x} thin films, *Physica B*, 2005, **370**, 264–276.

- 78 J. C. Manifacier, J. Gasiot and J. P. Fillard, A simple method for the determination of the optical constants n ; k and the thickness of a weakly absorbing thin film, *J. Phys. E: Sci. Instrum.*, 1976, **9**, 1002–1004.
- 79 D. A. G. Bruggeman, Berechnung verschiedener physikalischer Konstanten von heterogenen Substanzen I. Dielektrizitätskonstanten und Leitfähigkeiten der Mischkörper aus isotropen Substanzen, *Ann. Phys.*, 1935, **416**, 636–664.
- 80 G. E. Jellison and F. A. Modine, Parameterization of the optical functions of amorphous materials in the interband region, *Appl. Phys. Lett.*, 1996, **69**, 371–373; G. E. Jellison and F. A. Modine, Erratum: ‘Parameterization of the optical functions of amorphous materials in the interband region’, *Appl. Phys. Lett.*, 1996, **69**, 2137.
- 81 J. Pellicer-Porres, D. Martinez-Garcia, A. Segura, P. Rodriguez-Hernandez, A. Munoz, J. C. Chervin, N. Garro and D. Kim, Pressure and temperature dependence of the lattice dynamics of CuAlO_2 investigated by Raman scattering experiments and *ab initio* calculations, *Phys. Rev. B: Condens. Matter Mater. Phys.*, 2006, **74**, 184301.